

Structure of decay-accelerating factor bound to echovirus 7: A virus-receptor complex

Yongning He*, Feng Lin[†], Paul R. Chipman*, Carol M. Bator*, Timothy S. Baker*, Menachem Shoham[‡], Richard J. Kuhn*, M. Edward Medof[†], and Michael G. Rossmann*[§]

*Department of Biological Sciences, Purdue University, West Lafayette, IN 47907-1392; and [†]Institute of Pathology and [‡]Department of Biochemistry, Case Western Reserve University, Cleveland, OH 44106

Edited by Peter Palese, Mount Sinai School of Medicine, New York, NY, and approved May 29, 2002 (received for review March 19, 2002)

Echoviruses are enteroviruses that belong to *Picornaviridae*. Many echoviruses use decay-accelerating factor (DAF) as their cellular receptor. DAF is a glycosylphosphatidylinositol-anchored complement regulatory protein found on most cell surfaces. It functions to protect cells from complement attack. The cryo-electron microscopy reconstructions of echovirus 7 complexed with DAF show that the DAF-binding regions are located close to the icosahedral twofold axes, in contrast to other enterovirus complexes where the viral canyon is the receptor binding site. This novel receptor binding position suggests that DAF is important for the attachment of viral particles to host cells, but probably not for initiating viral uncoating, as is the case with canyon-binding receptors. Thus, a different cell entry mechanism must be used for enteroviruses that bind DAF.

Echoviruses (ECHO) are small, nonenveloped, positive-strand RNA viruses (1) that belong to the *Enterovirus* genus of *Picornaviridae*. Picornavirus capsids have 60 copies each of four viral proteins: VP1, VP2, VP3, and VP4. These proteins form an icosahedral shell with an ≈ 300 -Å external diameter that encapsidates an ≈ 7.5 -kb RNA genome. ECHOs have ≈ 31 serotypes (1) and can cause aseptic meningitis in humans and other hosts. Among enteroviruses, ECHOs have the greatest genomic and structural similarity to coxsackieviruses. The crystal structures of ECHO1 (2), coxsackievirus B3 (CVB3) (3), and coxsackievirus A9 (4) show that they have features similar to other enteroviruses and rhinoviruses.

An important surface feature of the enterovirus and rhinovirus capsid is a narrow depression around each of the fivefold axes termed the canyon, which was predicted to be the receptor binding site for picornaviruses (5). This hypothesis was confirmed by cryo-electron microscopy (cryoEM) reconstruction of human rhinoviruses 14 and 16 (HRV14 and HRV16) complexed with intracellular adhesion molecule-1 (ICAM-1 or CD54) (6, 7), poliovirus (Mahoney) complexed with poliovirus receptor (CD155) (8–10), coxsackievirus A21 complexed with ICAM-1 (11), and CVB3 complexed with coxsackievirus-adenovirus receptor (CAR) (12). Conservation of receptor binding within the canyon, despite the evolutionary divergence of these viruses, suggests that this binding site might provide an evolutionary advantage. One such advantage is that, during viral entry, the site may be required for triggering uncoating (13, 14). In contrast, binding of HRV2 to very low-density lipoprotein receptor (VLDL-R) does not destabilize the virus. Consistent with the above proposition, the cryoEM reconstruction indicated that VLDL-R binds around the fivefold axes, not in the canyons (15). It is noteworthy that VLDL-R does not belong to the Ig superfamily (IgSF), unlike all of the other canyon-binding receptors.

Many serotypes (nos. 3, 6, 7, 11, 12, 13, 19, 21, 24, 25, 29, 30, and 33) of ECHOs use decay-accelerating factor (DAF, CD55) as their cellular receptor (16–18), whereas other ECHOs (nos. 1 and 8) bind very late antigen (VLA-2) integrin (19). Recent studies (20) indicate that DAF may not be the only receptor for ECHOs because it cannot convert virions into altered (A)

particles and because its binding to ECHOs is reversible. Some B group coxsackieviruses also have DAF binding activity while retaining binding activity to CAR (21–23). Thus, DAF is likely to act as an attachment receptor preliminary to viral cell entry.

DAF is a member of the complement control protein family, also termed regulators of complement activation (24). DAF is a glycosylphosphatidylinositol-anchored protein found on most cell surfaces. It dissociates self-cell-bound C3 convertases, C4b2a and C3bBb, at the early stage of the complement amplification cascade, thereby protecting self-cells from complement attack. Its extracellular region contains four 60-aa short consensus repeat (SCR) domains, also known as complement control protein (CCPⁿ) domains, followed by a 97-aa *O*-glycosylation-rich region (25) (Fig. 1). Molecules that contain SCR domains whose three-dimensional structures have been determined include a fragment of CD46 (used by measles viruses as a receptor), containing two SCR domains (26), and the vaccinia virus complement protein (VCP) that has four SCR domains (27).

Here, we report the structure of ECHO7 complexed with DAF determined by cryoEM image analysis. The structure shows that DAF binds close to the icosahedral twofold axes on the viral surface, rather than binding into the canyon. This finding suggests that DAF has a different role in cell entry compared with Ig-like cellular receptors of enteroviruses and, hence, that a different cell entry mechanism may be used for enteroviruses that bind DAF.

Methods

Virus and DAF Purification. The inoculum of ECHO7 (Wallace) was purchased from the American Type Culture Collection and grown in rhabdomyosarcoma (RD) cells. ECHO7 was purified by sedimentation through a 30% sucrose cushion and then through a 7.5–45% sucrose gradient (28). The final concentration of virus for cryoEM was 4 mg/ml.

Different human DAF SCR modules were expressed in *Pichia pastoris* as C-terminal His-tagged proteins and purified by Ni²⁺ affinity chromatography. Briefly, DNAs coding for SCR1,2,3,4, SCR2,3,4, and SCR2,3 were amplified by PCR using human DAF cDNAs as templates. After sequencing to confirm the accuracy of the DNA sequences, the different SCR modules were cloned into the plasmid pPICZaA so as to yield expression constructs. After selection of high-level expression colonies of transformed *Pichia* strain SMD 1168, upon methanol induction

This paper was submitted directly (Track II) to the PNAS office.

Abbreviations: CAR, coxsackievirus-adenovirus receptor; CVB3, coxsackievirus B3; cryoEM, cryo-electron microscopy; DAF, decay-accelerating factor; ECHO, echovirus; HRV, human rhinovirus; IgSF, immunoglobulin superfamily; RD, rhabdomyosarcoma; SCR, short consensus repeat; VCP, virus complement protein; VLDL-R, very low-density lipoprotein receptor; VP, viral protein.

Data deposition: The atomic coordinates of the fitted DAF molecules have been deposited in the Protein Data Bank, www.rcsb.org (PDB ID code 1M11).

[§]To whom reprint requests should be addressed. E-mail: mgr@indiana.bio.purdue.edu.

[†]The more recent nomenclature is CCP domain. However, as most authors still use SCR domain, we shall retain the older name in this paper.

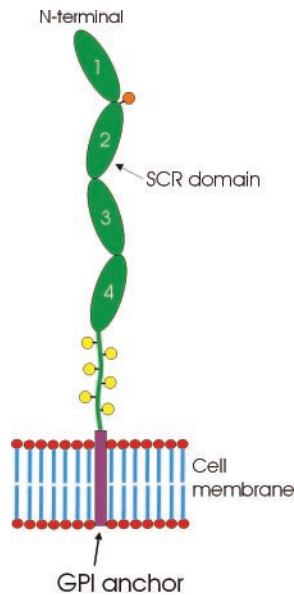


Fig. 1. Diagrammatic structure of DAF. The green ellipses represent the SCR domains. The yellow spheres are O-linked and the orange spheres are N-linked carbohydrate moieties. GPI, glycosylphosphatidylinositol.

each DAF SCR product was expressed and secreted into the medium. Secreted products were purified by Ni²⁺ affinity chromatography, elution fractions were dialyzed against PBS, and protein was quantified (29, 30).

Plaque Reduction. Monolayers of RD cells were grown in 60-mm culture dishes. ECHO7 inoculum was diluted in PBS to reduce the plaque-forming units by a factor of 10⁸. Different DAF SCR modules were added to the diluted virus and incubated in microcentrifuge tubes for 2 h at room temperature. Media were aspirated from each dish and monolayers were infected with 0.2 ml of diluted virus and DAF fragments. Virus was allowed to attach to the cells for 30 min at room temperature. Cultures were then fed with media containing 0.8% agar and incubated at 37°C for 24 h. Cells were stained with neutral red to visualize plaques.

CryoEM Reconstruction. The DAF samples were incubated with ECHO7 at 4°C with a ratio of 300:1. Small aliquots (≈3.5 μl) of this mixture were applied to carbon-coated electron microscope grids and vitrified in liquid ethane as described by Baker *et al.* (31). A control sample of ECHO7 by itself was prepared similarly. Electron micrographs were recorded on Kodak SO-163

film by using a Philips CM300 FEG microscope. Micrographs were digitized with a Zeiss PHODIS microdensitometer at 14-μm intervals, corresponding to 3.1 Å on the specimen (Table 1).

A cryoEM reconstruction of CVB3 was used as an initial model for determining particle orientations and centers by means of the polar Fourier transform method (31, 32). Corrections to compensate for the effects of the microscope contrast transfer function were applied in the reconstruction procedure. The resolution of the resultant three-dimensional image reconstructions (Table 1) was estimated by splitting the image data into two sets and comparing the structure factors obtained in separate reconstructions.

Model Fitting. The capsid protein sequences of CVB3 and ECHO1 possess ≈75% similarity with ECHO7. The crystal structure of CVB3 (Protein Databank ID code 1COV) (3) was used as a homologous structure for ECHO7. VCP, which has 25% sequence identity with DAF1234, was used as a homologous model for DAF. A difference map was calculated between the observed cryoEM density of the complex and ECHO7, thus isolating the density corresponding to DAF. The VCP model was used to interpret the DAF difference density by using the program o (33). Because the density corresponding to DAF is a combination of two equal binding orientations related by 180°, the hand-fitting operation was somewhat uncertain.

The footprint of DAF on ECHO7 was determined by the program EMFIT (34, 35). The model of ECHO7 was placed into the ECHO7–DAF cryoEM density. The density of ECHO7 was then removed by setting to zero every grid point within a radius of 2.0 Å of each ECHO7 atom, leaving the density of DAF. The residues of ECHO7 in contact with DAF were then identified by taking the average density of all grid points within a radius of 3.4 Å around each ECHO7 atom. Thus, the atoms with relatively large average densities were those that were close to the remaining DAF density. This procedure avoided the use of an inaccurate DAF model, but instead used the much better defined ECHO7 structure.

Results and Discussion

The cryoEM reconstruction of ECHO7 complexed with DAF1234 (domain SCR1–4) or DAF234 (domain SCR2–4) (Fig. 2) showed that DAF binds across icosahedral twofold axes on the viral surface, not in the canyons, as is the case for other enterovirus and major rhinovirus receptor complexes (6–12), nor around the icosahedral fivefold axes, as is the case for the HRV2–VLDL-R complex (15). The density corresponding to DAF in the ECHO7–DAF1234 and ECHO7–DAF234 complexes is quite low (25% and 15%, respectively) relative to the density of the viral capsids. Consistent with the results of the cryoEM reconstructions, the efficiency of plaque inhibition by

Table 1. Statistics of the cryoEM reconstructions

Sample	No. of micrograph	Incubation time, min	Defocus,* μm	Magnification	Dose, e ⁻ /Å ²	No. of particles, selected/total	Correlation coefficient [†]	Resolution,* Å
ECHO7–DAF1234 complex	22	120	1.8–4.2	45,000	16.6	1,363/2,817	0.335	16
ECHO7–DAF234 complex	19	120	1.8–4.1	45,000	17.3	1,108/2,380	0.383	18
ECHO7	10	—	1.7–4.4	45,000	16.5	554/1,138	0.425	16

*Determined from phase contrast transfer function of the microscope.

[†]Real-space correlation coefficient (CC) for selected particles,

$$CC = \frac{\sum[(r\rho_i)(r\rho_m) - \langle r\rho_i \rangle \langle r\rho_m \rangle]}{\left\{ \sum[(r\rho_i)^2 - \langle r\rho_i \rangle^2] \sum[(r\rho_m)^2 - \langle r\rho_m \rangle^2] \right\}^{1/2}}$$

In this equation, ρ_i is the electron density of the boxed cryoEM image, ρ_m is the electron density of the model projection, and r is the radius of the corresponding density point, which assures proper weighting of the densities. The angle brackets indicate mean values.

[†]Resolution at which the correlation between two independent three-dimensional reconstructions falls below 0.5.

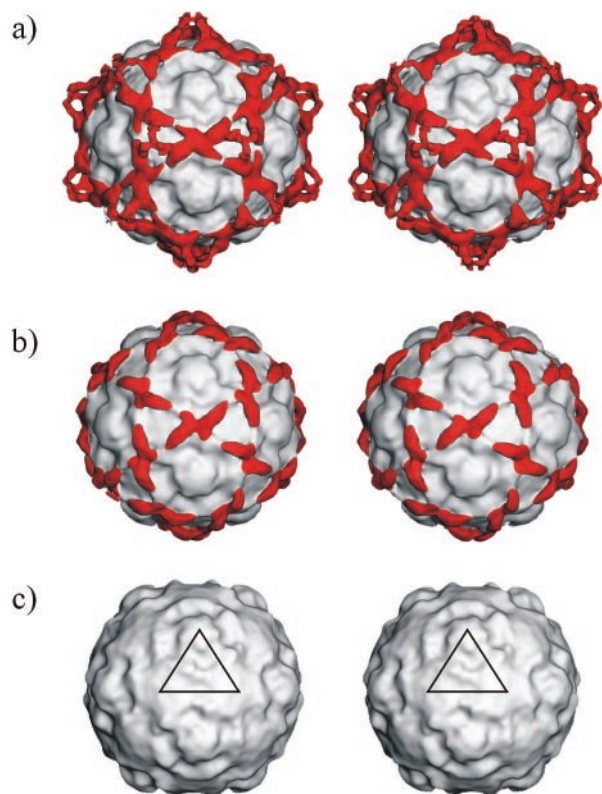


Fig. 2. Surface representation of cryoEM image reconstructions. Comparison of ECHO7 (c) with complexes of ECHO7 and DAF fragments shows (in red) the density attributed to DAF. An icosahedral asymmetric unit is outlined in black in c. Comparisons of the reconstruction of ECHO7 complexed with either DAF1234 (a) or DAF234 (b) shows that SCR domain 1 is located near the threefold axes. The surface contour is at 1σ for each complex.

the progressively truncated forms of DAF protein varied (36) in the order of DAF1234 ($\approx 85\%$) > DAF234 ($\approx 65\%$) > DAF23 ($\approx 30\%$). The low occupancy of DAF in the viral DAF complexes suggests that the binding affinity of soluble DAF to ECHO7 is quite low. This finding contrasts with canyon-binding receptors, such as CAR, poliovirus receptor, and intracellular adhesion molecule-1, all of which have high occupancy in their corresponding virus-receptor complexes. Considering the similarities among enteroviruses and the fact that DAF binds reversibly to ECHO7 (20), DAF might be an attachment receptor, suggesting that a secondary receptor is required to target the canyon with higher binding affinity for viral uncoating.

The N-terminal SCR domain (SCR1) of DAF1234 can be clearly recognized by comparing the reconstruction of the ECHO7/DAF1234 and ECHO7/DAF234 complexes (Fig. 2). SCR1 is located close to the icosahedral threefold axes and might form trimeric associations of DAF molecules bound to neighboring twofold axes. The trimerization of SCR1 visualized in the ECHO7/DAF1234 complex may be artifactual because of the icosahedral threefold averaging applied during the cryoEM reconstruction, whereas, in reality, one or two of the DAF molecules might be missing at any one trimeric vertex. Although the SCR domains are close to the viral surface, the large, flexible, O-linked glycosylation region will provide ample space between the virus and the cell membrane, in a manner equivalent to that found for the multidomain IgSF molecules.

A homologue of DAF with known atomic structure is VCP (27). VCP has 25% sequence identity with DAF and has four SCR domains forming an extended W-shape structure. The length of each SCR domain is about 30 Å. The four linked SCR

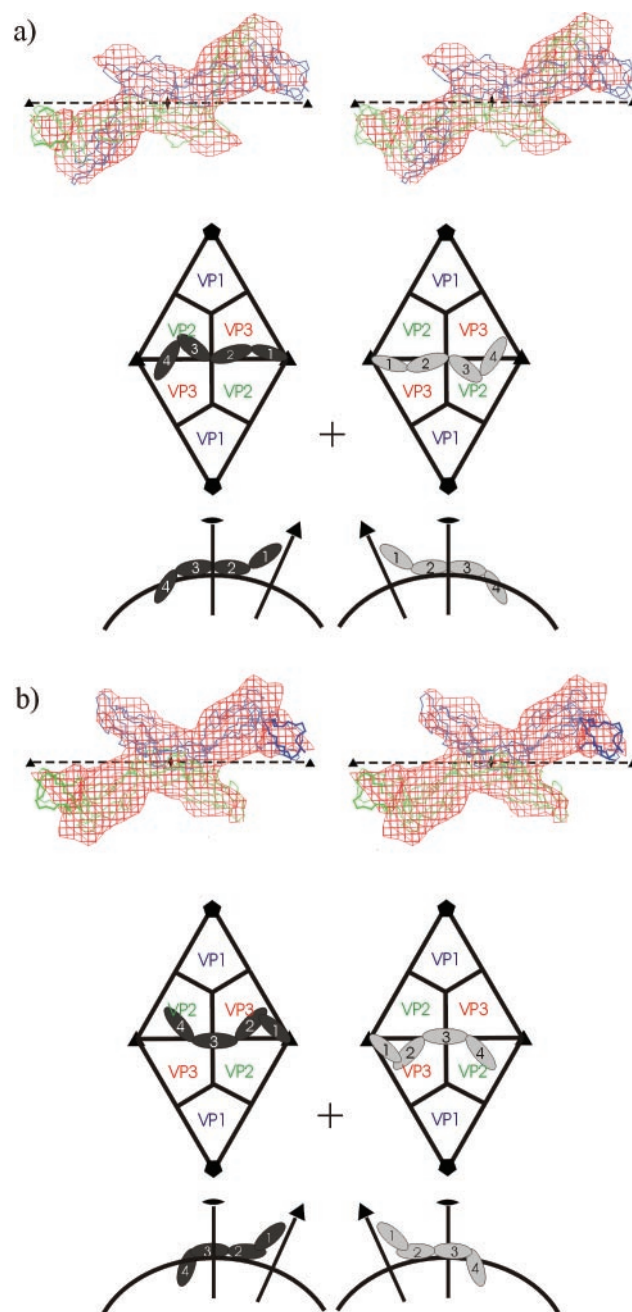


Fig. 3. Alternative interpretations (a and b) of the DAF difference density (orange) in terms of possible DAF structures. Both interpretations are represented by three views. The difference density fitted with the DAF model viewed down an icosahedral twofold axis is shown at the top in each case. The middle and bottom views show diagrammatic top and side views of two icosahedral asymmetric units of the virus with bound DAF represented by four SCR domains in black and gray. The middle view also shows the position of VP1, VP2, and VP3. The positions of fivefold, threefold, and twofold axes are indicated by pentagons, triangles, and ellipses, respectively, in the middle and bottom views.

domains of VCP could be fitted into the DAF difference density of the ECHO7-DAF1234 cryoEM reconstruction, taking into account the site identified as SCR1. This process required some hinge adjustments between domains. Two alternative domain arrangements were possible (Fig. 3), although in both cases the DAF molecules related by icosahedral twofold axes were in steric collision. Presumably, only one of the two DAF molecules would

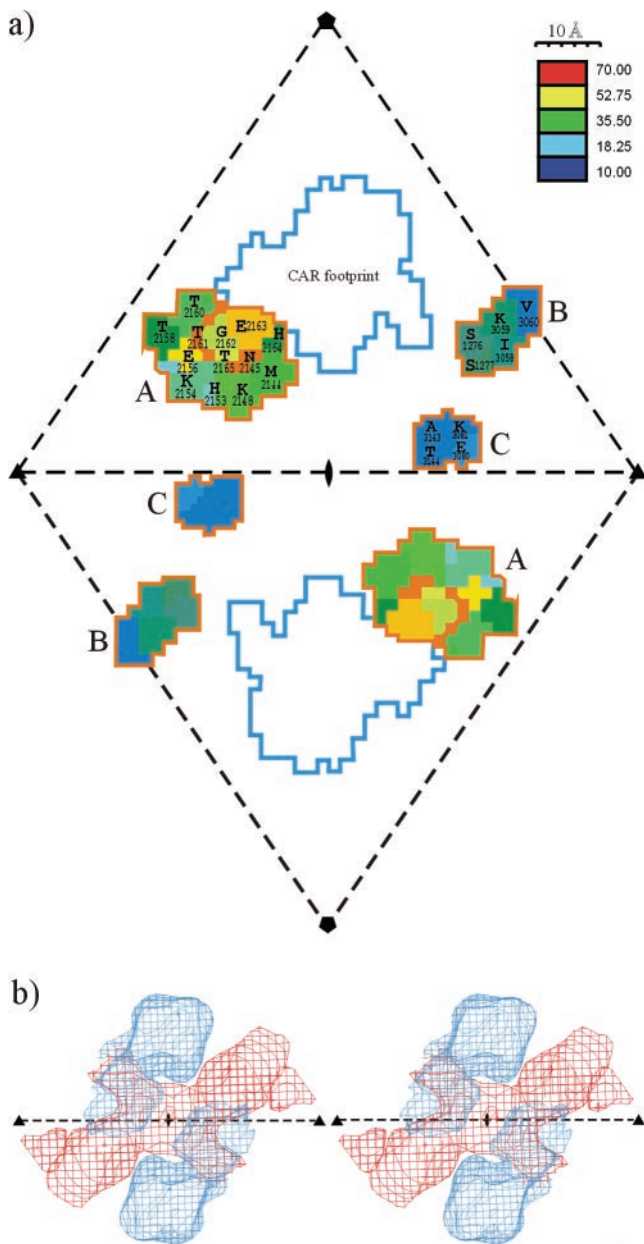


Fig. 4. (a) Two icosahedral asymmetric units showing the footprints of CAR (blue outline) and DAF (orange outline) on ECHO7. The color scale corresponds to the height of the DAF density close to the surface of the virus. Thus, large values (red) correspond to close contacts between DAF and the virus. Amino acids in the contact region are identified by an amino acid sequence number (VP2 is 2000+, VP3 is 3000+) and a one-letter residue amino acid code derived from the SwissProt AY 036579 sequence. (b) A stereo diagram showing the superposition of the EM difference densities of CAR (blue) bound to CVB3 and DAF (orange) bound to ECHO7.

be able to bind across the twofold axes, and the two possible orientations would be randomly distributed among the 30 sites on each virus particle. Thus, the DAF density obtained from cryoEM is an average of two binding orientations (Fig. 3). One of these models (Fig. 3b) was similar to a predicted structure of DAF (25).

The viral amino acid residues that are in contact with the DAF receptor molecules were determined as described in *Methods*. The binding interface of DAF on the viral surface was found to be composed of regions A, B, and C (Fig. 4). Region A, the

Table 2. Contact between DAF SCR domains and the viral surface for the two likely fits (a and b) of the DAF structure to the DAF difference density

VP	Region	Fit (a)	Fit (b)
VP2	A	SCR3	SCR4
VP3	B	SCR4	SCR2
VP3	C	SCR2	SCR2–SCR3

largest contact region, is formed by the hypervariable “puff” sequence of VP2 associated with the NIm-II binding site for neutralizing antibodies in HRV14 (5) and is located outside the south rim of the canyon. Region B includes the hypervariable “knob” residues associated with the NIm-III binding site for neutralizing antibodies in HRV14 (5). Thus, the non-IgSF receptors DAF and VLDL-R bind to regions of high surface variability and sites used by neutralizing antibodies, NIm-I to VLDL-R and NIm-II and NIm-III to DAF. It may not be surprising, therefore, that there are fewer minor-group HRVs and echoviruses, respectively, as these viruses do not appear to have a mechanism to escape host immune surveillance.

The major contacts of DAF are between SCR2, SCR3, and SCR4 with VP2 and VP3 (Table 2), whereas SCR1 does not contact the viral surface for either structural model. Both possible DAF models (and the area of the contact regions) are roughly consistent with a kinetic study (28), which indicated that the order of contribution of SCR binding on ECHO11 is SCR3 > SCR2 and SCR4 > SCR1, although the model in Fig. 3a seems to be in slightly better agreement.

In light of the variable occupancy of DAF on the viral surface and the random selection of two binding orientations at the same binding site, it is unlikely that an ECHO7–DAF complex is crystallizable. Thus, a cryoEM reconstruction is likely to be the only way of determining the site of interaction of the receptor with the virus.

Considering the similarities of CVB3 and ECHO7, it is reasonable to assume that the CVB3 will bind to DAF in a similar way as does ECHO7. One variant of CVB3 that is adapted to RD cells uses DAF as its cellular receptor (37). There are two differences in VP2 (D2018V and T2151S, see Fig. 4 for sequence number nomenclature) between non-DAF-binding CVB3 (Nancy) and DAF-binding CVB3 (RD) (38). Neither of these two residues are in the CAR binding footprint: residue 2108 is an internal residue and located on β D of VP2, and residue 2151 (roughly equivalent to ECHO7 H2153) is located on the surface within the DAF binding region A (Fig. 4), demonstrating the importance of this residue for DAF binding.

CVB3 normally use CAR as their cellular receptor. However, many CVB3 also have DAF binding activity (21, 23, 37). A study of a CVB3 variant, grown in RD cells, had shown that it requires both CAR and DAF for lytic infection (22), and another study had indicated that a CVB3 that binds DAF uses CAR for entry into pig cells (39). These observations indicate that CVB3 can bind CAR and DAF on the viral surface simultaneously, although full occupancy may not be required for both types of receptor molecules. The footprint of CAR on the surface of CVB3 (12) maps into the canyon, but it does not overlap with the footprint of DAF (Fig. 4) (assuming DAF binds to CVB3 in a similar way as it does to ECHO7 as suggested by the mutational data), except along the edge of the south rim of the canyon. In addition, the densities of CAR complexed to CVB3 and DAF complexed to ECHO7 do not overlap (Fig. 4). This finding suggests that both CAR and DAF might be able to bind to CVB3, forming a ternary complex. Nevertheless, the binding affinity of DAF and CAR might slightly interfere with each other because

a few residues are involved in both of the footprints along the south rim of canyon. Furthermore, considering the binding geometry of CAR and DAF on the viral surface, the virion should bind DAF before CAR, for otherwise the DAF molecule might not be able to pass through the narrow space underneath the twofold-related CAR molecules. Because DAF is expressed in all cell types, usually with a greater concentration per unit surface area than other receptor molecules on cell surfaces, it is likely that virions bind to DAF first. Therefore, this sequence of events would increase the binding opportunities for the secondary receptor that initiates uncoating, consistent with the role of DAF being an attachment receptor.

Among the known picornavirus-receptor complexes, all of the canyon-binding receptors, intracellular adhesion molecule-1, poliovirus receptor, and CAR, belong to the IgSF. In contrast, the two non-IgSF receptors, VLDL-R and DAF, are noncanyon-

binding receptors. Thus, the Ig domain may have some advantages when binding into the canyon compared with other protein folds. Furthermore, the Ig receptors irreversibly destabilize the virus, necessitating considerable care in the timing and temperature for performing cryoEM experiments on virus-receptor complexes. In contrast, picornaviruses appear to be quite stable upon binding to VLDL-R or DAF. This finding indicates that the Ig domains are suitable triggers that activate a conformational switch in the canyon that initiates uncoating.

We thank Wei Zhang, Chuan (River) Xiao, Suchetana (Tuli) Mukhopadhyay, and Xing Zhang for helpful discussions and Cheryl Towell and Sharon Wilder for preparation of the manuscript. This work was supported by National Institutes of Health Grants AI11219 (to M.G.R.), AI23598 (to M.E.M.), and GM33050 (to T.S.B.), the Keck Foundation for the purchase of the CM300 FEG microscope, and a reinvestment grant from Purdue University.

- Pallansch, M. A. & Roos, R. P. (2001) in *Fields Virology*, ed. Howley, P. M. (Lippincott Williams and Wilkins, Philadelphia), Vol. 1, pp. 723–775.
- Filman, D. J., Wien, M. W., Cunningham, J. A., Bergelson, J. M. & Hogle, J. M. (1998) *Acta Crystallogr. D* **54**, 1261–1272.
- Muckelbauer, J. K., Kremer, M., Minor, I., Diana, G., Dutko, F. J., Groarke, J., Pevear, D. C. & Rossmann, M. G. (1995) *Structure (London)* **3**, 653–667.
- Hendry, E., Hatanaka, H., Fry, E., Smyth, M., Tate, J., Stanway, G., Santti, J., Maaronen, M., Hyypia, T. & Stuart, D. (1999) *Structure (London)* **7**, 1527–1538.
- Rossmann, M. G., Arnold, E., Erickson, J. W., Frankenberger, E. A., Griffith, J. P., Hecht, H. J., Johnson, J. E., Kamer, G., Luo, M., Mosser, A. G., et al. (1985) *Nature (London)* **317**, 145–153.
- Olson, N. H., Kolatkar, P. R., Oliveira, M. A., Cheng, R. H., Greve, J. M., McClelland, A., Baker, T. S. & Rossmann, M. G. (1993) *Proc. Natl. Acad. Sci. USA* **90**, 507–511.
- Kolatkar, P. R., Bella, J., Olson, N. H., Bator, C. M., Baker, T. S. & Rossmann, M. G. (1999) *EMBO J.* **18**, 6249–6259.
- He, Y., Bowman, V. D., Mueller, S., Bator, C. M., Bella, J., Peng, X., Baker, T. S., Wimmer, E., Kuhn, R. J. & Rossmann, M. G. (2000) *Proc. Natl. Acad. Sci. USA* **97**, 79–84.
- Belnap, D. M., McDermott, B. M., Jr., Filman, D. J., Cheng, N., Trus, B. L., Zuccola, H. J., Racaniello, V. R., Hogle, J. M. & Steven, A. C. (2000) *Proc. Natl. Acad. Sci. USA* **97**, 73–78.
- Xing, L., Tjarnlund, K., Lindqvist, B., Kaplan, G. G., Feigelstock, D., Cheng, R. H. & Casasnovas, J. M. (2000) *EMBO J.* **19**, 1207–1216.
- Xiao, C., Bator, C. M., Bowman, V. D., Rieder, E., He, Y., Hébert, B., Bella, J., Baker, T. S., Wimmer, E., Kuhn, R. J. & Rossmann, M. G. (2001) *J. Virol.* **75**, 2444–2451.
- He, Y., Chipman, P. R., Howitt, J., Bator, C. M., Whitt, M. A., Baker, T. S., Kuhn, R. J., Anderson, C. W., Freimuth, P. & Rossmann, M. G. (2001) *Nat. Struct. Biol.* **8**, 874–878.
- Rossmann, M. G. (1994) *Protein Sci.* **3**, 1712–1725.
- Oliveira, M. A., Zhao, R., Lee, W., Kremer, M. J., Minor, I., Rueckert, R. R., Diana, G. D., Pevear, D. C., Dutko, F. J., McKinlay, M. A. & Rossmann, M. G. (1993) *Structure (London)* **1**, 51–68.
- Hewat, E. A., Neumann, E., Conway, J. F., Moser, R., Ronacher, B., Marlovits, T. C. & Blaas, D. (2000) *EMBO J.* **19**, 6317–6325.
- Bergelson, J. M., Chen, M., Solomon, K. R., St. John, N. F., Lin, H. & Finberg, R. W. (1994) *Proc. Natl. Acad. Sci. USA* **91**, 6245–6248.
- Ward, T., Pipkin, P. A., Clarkson, N. A., Stone, D. M., Minor, P. D. & Almond, J. W. (1994) *EMBO J.* **13**, 5070–5074.
- Powell, R. M., Schmitt, V., Ward, T., Goodfellow, I., Evans, D. J. & Almond, J. W. (1998) *J. Gen. Virol.* **79**, 707–713.
- Bergelson, J. M., Shepley, M. P., Chan, B. M. C., Hemler, M. E. & Finberg, R. W. (1992) *Science* **255**, 1718–1720.
- Powell, R. M., Ward, T., Evans, D. J. & Almond, J. W. (1997) *J. Virol.* **71**, 9306–9312.
- Bergelson, J. M., Modlin, J. F., Wieland-Alter, W., Cunningham, J. A., Crowell, R. L. & Finberg, R. W. (1997) *J. Infect. Dis.* **175**, 697–699.
- Shafren, D. R., Williams, D. T. & Barry, R. D. (1997) *J. Virol.* **71**, 9844–9848.
- Martino, T. A., Petric, M., Brown, M., Aitken, K., Gauntt, C. J., Richardson, C. D., Chow, L. H. & Liu, P. P. (1998) *Virology* **244**, 302–314.
- Reid, K. B. M. & Day, A. J. (1989) *Immunol. Today* **10**, 117–180.
- Kuttner-Kondo, L., Medof, M. E., Brodbeck, W. & Shoham, M. (1996) *Protein Eng.* **9**, 1143–1149.
- Casasnovas, J. M., Larvie, M. & Stehle, T. (1999) *EMBO J.* **18**, 2911–2922.
- Murthy, K. H., Smith, S. A., Ganesh, V. K., Judge, K. W., Mullin, N., Barlow, P. N., Ogata, C. M. & Kotwal, G. J. (2001) *Cell* **104**, 301–311.
- Lea, S. M., Powell, R. M., McKee, T., Evans, D. J., Brown, D., Stuart, D. I. & van der Merwe, P. A. (1998) *J. Biol. Chem.* **273**, 30443–30447.
- Lin, F., Immormino, R. M., Shoham, M. & Medof, M. E. (2001) *Arch. Biochem. Biophys.* **393**, 67–72.
- Lin, F., Fukuoka, Y., Spicer, A., Ohta, R., Okada, N., Harris, C. L., Emancipator, S. N. & Medof, M. E. (2001) *Immunology* **104**, 215–225.
- Baker, T. S., Olson, N. H. & Fuller, S. D. (1999) *Microbiol. Mol. Biol. Rev.* **63**, 862–922.
- Baker, T. S. & Cheng, R. H. (1996) *J. Struct. Biol.* **116**, 120–130.
- Jones, T. A., Zou, J. Y., Cowan, S. W. & Kjeldgaard, M. (1991) *Acta Crystallogr. A* **47**, 110–119.
- Rossmann, M. G. (2000) *Acta Crystallogr. D* **56**, 1341–1349.
- Rossmann, M. G., Bernal, R. & Pletnev, S. V. (2001) *J. Struct. Biol.* **136**, 190–200.
- Powell, R. M., Ward, T., Goodfellow, I., Almond, J. W. & Evans, D. J. (1999) *J. Gen. Virol.* **80**, 3145–3152.
- Bergelson, J. M., Mohanty, J. G., Crowell, R. L., St. John, N. F., Lublin, D. M. & Finberg, R. W. (1995) *J. Virol.* **69**, 1903–1906.
- Lindberg, A. M., Crowell, R. L., Zell, R., Kandolf, R. & Pettersson, U. (1992) *Virus Res.* **24**, 187–196.
- Spiller, O. B., Goodfellow, I. G., Evans, D. J., Hinchliffe, S. J. & Morgan, B. P. (2002) *J. Gen. Virol.* **83**, 45–52.